Rydberg-Mediated Entanglement in a Two-Dimensional Neutral Atom Qubit Array

T. M. Graham, M. Kwon, B. Grinkemeyer, Z. Marra, X. Jiang, M. T. Lichtman,* Y. Sun,† M. Ebert,‡ and M. Saffman‡

Department of Physics, University of Wisconsin-Madison, 1150 University Avenue, Madison, Wisconsin 53706, USA

(Received 16 August 2019; published 4 December 2019)

We demonstrate high fidelity two-qubit Rydberg blockade and entanglement on a pair of sites in a large two-dimensional qubit array. The qubit array is defined by a grid of blue detuned lines of light with 121 sites for trapping atomic qubits. Improved experimental methods have increased the observed Bell state fidelity to $F_{\mathrm{Bell}} = 0.86(2)$. Accounting for errors in state preparation and measurement we infer a fidelity of $F_{\mathrm{Bell}}^{\text{-SPAM}} = 0.88$. Accounting for errors in single qubit operations we infer that a Bell state created with the Rydberg mediated C_Z gate has a fidelity of $F_{\mathrm{Bell}}^{C_Z} = 0.89$. Comparison with a detailed error model based on quantum process matrices indicates that finite atom temperature and laser noise are the dominant error sources contributing to the observed gate infidelity.

DOI: 10.1103/PhysRevLett.123.230501

Achieving the promise of a computational advantage for quantum machines is predicated on the development of approaches that combine a large number of qubits with a high fidelity universal gate set. A broad range of experimental platforms for quantum computing are being developed [1] and very high fidelity two-qubit gates have been implemented in trapped ion and superconducting systems with small numbers of qubits: $F_{\mathrm{Bell}} \geq 0.999$ with two trapped ions [2] and a phase gate fidelity $F_{C_Z} > 0.99$ with five superconducting qubits [3]. As the number of qubits in a quantum computer is scaled up, crosstalk and undesired interactions limit fidelity. Average Bell state fidelities of $F_{\mathrm{Bell}} = 0.975$ were obtained in an 11 qubit ion trap [4]. An approach based on encoding in hyperfine states of optically trapped neutral atoms holds great promise for scaling qubit number without limiting gate fidelities. The physical attribute that enables scaling with low crosstalk is the separation by 12 orders of magnitude between the weak coupling strength of neutral atom hyperfine qubits, and the strong interactions of Rydberg excited atoms [5] that enable entangling gates [6]. We report here on experimental progress in achieving high two-qubit entanglement fidelity in a 2D array. This gate was performed on atoms occupying just two trap sites in the full array. However, because a large grid of qubits (121 traps with an average of 55% loading) was used, the architecture is compatible with scaling to algorithms involving many qubits. The Bell state fidelity of $F_{\mathrm{Bell}}^{C_Z} = 0.89$, together with previously demonstrated single qubit gates with $F > 0.99$ [7,8], and atom rearrangement capabilities [9], suggest that neutral atom arrays will soon be capable of advancing the state of the art in gate based quantum computing.

A computationally universal quantum gate set can be built from one- and two-qubit operations on neutral atom qubits. One-qubit gates with fidelities determined by randomized benchmarking exceeding 0.99 and intersite crosstalk less than 0.01 have been demonstrated in 2D [7] and 3D [8] arrays of neutral atom qubits. However, the fidelity of two-qubit entangling gates has been limited to much lower values. The highest fidelity results from the last few years for entanglement of pairs of neutral atoms are 0.79 [10], 0.81 [11], 0.59 [12], 0.81 [13]. These fidelity numbers are corrected for state preparation and measurement (SPAM) errors and in some cases also atom loss. Recently, qubits encoded in one hyperfine ground state and one Rydberg state were demonstrated with entanglement fidelity of 0.97 [14], although Rydberg encoding limits the coherence time to < 0.1 ms, much shorter than the seconds of coherence time demonstrated with qubits encoded in hyperfine ground states [8,15].

The experimental setup is an upgraded version of that described in Ref. [10]. A two-dimensional array of Cs atoms is prepared using a projected optical lattice with period $d = 3.1(1)$ μm (numbers in parentheses are uncertainties in the last digit) and wavelength $\lambda = 825$ nm. (see Fig. 1). In contrast to our previous work with a Gaussian beam array [16], the array structure is defined by a square grid of lines of light prepared using diffractive optical elements [17]. Each unit cell provides 3D atom confinement with transverse localization due to the repulsive walls of blue-detuned light, and axial confinement perpendicular to the plane of the array provided by diffractive spreading of the lines. We measure vacuum limited lifetimes of ~30 s, longitudinal coherence times in the Cs clock states of $T_1 = 0.75$ s, and an average temperature of $T_a \simeq 15$ μK. This temperature implies a limit on the clock state coherence time of $T_2^* = 1.6$ ms due to motional variation of the trap light intensity.

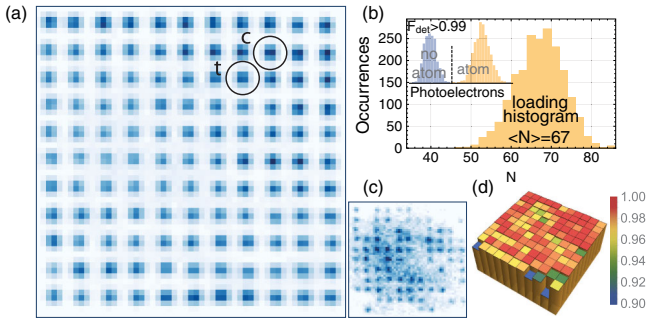

FIG. 1. Atomic qubit array. (a) Averaged fluorescence image of 121 site array after ICA processing with the control and target sites used for the presented data labeled. (b) Loading histogram showing an average filling fraction of 55% with inset showing state detection inferred after blow away of atoms in $f = 4$. Accounting for all 121 sites, the state detection error found from the overlap of Gaussians fitted to the $|0\rangle$ and $|1\rangle$ distributions was mean $= 0.014$, median $= 0.003$. (c) Single instance of atom loading. (d) Atom retention probability after measurement. The atom retention probability after two subsequent readout sequences was mean $= 96.9\%$, median $= 97.9\%$. The difference between mean and median is due to some sites on the edge of the array having lower retention due to optical aberrations.

The array is prepared by combining four laser sources with different frequencies such that the four beams defining each unit cell are separated by many MHz, but the frequencies are repeated in neighboring cells. With this configuration the structure and position of each trapping site are insensitive to phases from variations in optical path length. However, Talbot interference still occurs leading to additional trapping planes at axial separations of $L = 2(2d)^2/\lambda = 93$ μm. Detection of atoms in the array is hampered by scattering from atoms in the additional Talbot planes. We effectively reduce the background noise with regions of interest for each trap site determined using an independent component analysis (ICA) algorithm [17], see Fig. 1. Alternatively the Talbot planes can be eliminated by making each line a different frequency. We have implemented this using acousto-optic deflectors to generate arrays with up to 196 trapping sites and an average of 110 trapped atoms. Details of this approach will be given elsewhere [18].

The trapped Cs atoms are optically pumped into the clock states which form a qubit basis of $|0\rangle = |6s_{1/2}, f = 3, m_f = 0\rangle$ and $|1\rangle = |6s_{1/2}, f = 4, m_f = 0\rangle$. State $|1\rangle$ is resonantly coupled to the Rydberg state $|R\rangle = |66s_{1/2}, m_j = -1/2\rangle$ using a two-photon transition with counter-propagating $\lambda_1 = 459$ nm (σ_+) and $\lambda_2 = 1038$ nm (σ_-) laser beams which couple $6s_{1/2} \rightarrow 7p_{1/2} \rightarrow 66s_{1/2}$. We detune by $+680$ MHz from the center of mass of the $7p_{1/2}$ state and use a magnetic bias field of 0.6 mT directed along the quantization axis, which is collinear with the beam $\mathbf{k}$ vectors, to separate the Rydberg $m_j = \pm 1/2$ states. The choice of Rydberg principal quantum number is lower than in our previous demonstrations to minimize background electric field perturbations. With the small array period used here there is sufficient blockade strength and state lifetime at $n = 66$ that the resulting errors are minor contributions to the overall error model (see Table I below).

The Rydberg excitation beams are focused to beam waists ($1/e^2$ intensity radii) of $w_1 = w_2 = 3.0$ μm which are pointed to address desired array sites using two crossed acousto-optic modulators for each beam. Using acousto-optic modulators we address different array sites with

TABLE I. Error budget for Bell state preparation using experimental and calculated values. Individual error sources are combined by propagating the input state through a series of quantum processes using χ matrices [19].

Quantity	Error	Fidelity estimate
Atomic parameters and finite temperature effects		
Ground-Rydberg Doppler dephasing on control (calculated)	0.013	
Rydberg radiative lifetime on control (calculated)	0.0075	
Scattering $7p_{1/2}$ per atom per π pulse per Rydberg beam (calculated)	0.0012	
Blockade leakage (calculated)	0.001	
Atom position in Rydberg beams per atom per Rydberg π pulse (measured)	0.0025	
Laser noise per atom per π pulse (measured)	0.0025	
Rydberg crosstalk for $\|01\rangle$ (measured)	0.005	
Rydberg laser dephasing per atom per Rydberg π pulse (measured)	0.018 (nonblockaded)	
	0.006 (blockaded)	$F_{\text{Bell}}^{C_Z} = 0.887$
Single qubit errors		
Global per atom per μ wave $\pi/2$ pulses (4 total) (measured)	0.0028	
Stark-shift pulse (measured)	0.006	$F_{\text{Bell}}^{\text{SPAM}} = 0.877$
SPAM errors		
Readout loss per atom per readout (initial and final) (measured)	0.0025	
Optical pumping per atom (estimated)	0.005	
State measurement error per atom (measured)	0.000 15	$F_{\text{Bell}} = 0.853$

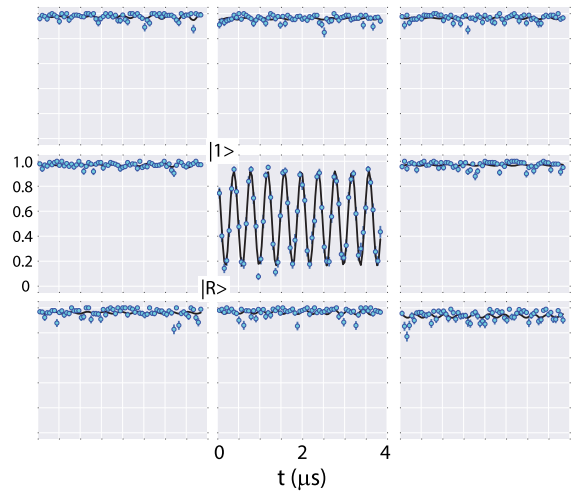

FIG. 2. Single site ground-Rydberg Rabi oscillations at $\Omega_R/2\pi = 2.5$ MHz with negligible crosstalk to the surrounding eight sites (see Ref. [19] for analysis). All atoms in the array were prepared in $|1\rangle$ directly before the targeted site was illuminated with Rydberg beams.

submicrosecond switching times which facilitates implementation of multiqubit algorithms. Figure 2 shows ground to Rydberg Rabi oscillation data in the array. The trap light is turned off during the Rydberg pulse. Since the blue detuned array traps Rydberg atoms when turned on again [34,35] there is only minimal mechanical loss of Rydberg states. A 9.2 GHz microwave pulse (duration 70 μs) was used to photoionize the Rydberg atom and improve detection efficiency to 80%–90%. Rydberg excitation was performed using diode lasers stabilized to high finesse optical resonators (~5 kHz linewidth) [19]. Phase noise of diode lasers has been shown to contribute to the decay of ground-Rydberg oscillations [20] and can be improved by resonator filtering [14]. Here we demonstrate comparable performance, without resonator filtering, but with careful tuning of the electronic Pound-Drever-Hall lock parameters to reduce the amplitude of servo bumps.

Fitting Rabi oscillations at the selected site in Fig. 2 does not reveal a statistically significant decay time. The radiative lifetime of the 66s state is 130 μs and the motional dwell time of a Rydberg atom in a trap site is ~50 μs. Both times are much longer than the observed 4 μs of coherent oscillations. However, the ground-Rydberg phase coherence decays due to Doppler sensitivity of the two-photon excitation according to [36] $\langle e^{i\phi}\rangle = e^{-t^2/T_{2,\mathrm{D}}^2}$ with $T_{2,\mathrm{D}} = \sqrt{2M_{\mathrm{Cs}}/k_B T_a}/k_{2\nu}$ and $k_{2\nu} = 2\pi/\lambda_1 - 2\pi/\lambda_2$. At $T_a = 15$ μK we find $T_{2,\mathrm{D}} = 6$ μs which would seem to imply a noticeable decay of the Rabi amplitude. This is not the case because the effective coherence, or persistence time, of a driven oscillation is longer than that of a static superposition of states [19].

The original proposal for a Rydberg C_Z gate [6] involves a sequence of three pulses connecting ground and Rydberg

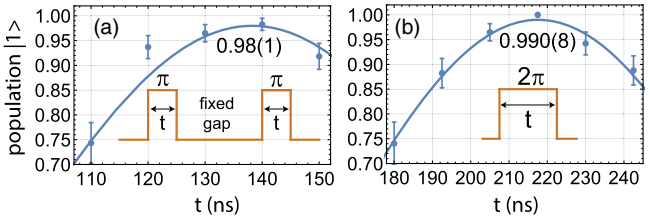

FIG. 3. Population in $|1\rangle$ after (a) control and (b) target qubit Rydberg pulses. The Rabi frequencies for the control and target pulses were $\Omega_R/2\pi = 3.6$ and 4.6 MHz, respectively, and gap time = 300 ns.

states: a π pulse on the control qubit, 2π on the target qubit, and π on the control qubit. It has been shown by detailed analysis of the atomic structure of the heavy alkalis that this pulse sequence is in principle capable of creating entanglement with fidelity $F > 0.998$ [21]. Many other Rydberg gate protocols have been proposed (see Ref. [37] for an overview). Using shaped pulses $F > 0.9999$ at gate times as short as 50 ns [38] appears possible. We report here on improved performance of the original proposal, leaving alternative protocols for future work.

A technical error that has been improved is the loss of Rydberg atoms after the π-gap-π pulses on the control qubit or the 2π pulse on the target qubit. These losses dominated error budgets in most earlier experiments [10,22,23]. Laser noise, optical beam quality, and alignment improvements have reduced population losses to 2% as shown in Fig. 3. To minimize excitation of Rydberg hyperfine states with $m_f \neq 0$ we align the $\mathbf{k}$ vectors of the 459 and 1038 nm beams to be antiparallel and set the background magnetic fields and polarization of the 459 nm beam to be accurately σ_+ relative to a quantization axis along $\mathbf{k}$. This is done by preparing the state $|4,4\rangle$ and minimizing the scattering rate due to the 459 nm light. For the data in Figs. 3–5, the beam waists were reduced to $w_1 = 2.25$ μm, $w_2 = 2.5$ μm to minimize crosstalk between sites.

To tune the conditional phase induced by a 2π Rydberg pulse we use a Ramsey sequence of $\pi/2$-gap-$(\pi/2)_\theta$ pulses on the qubit states (the last pulse is about an axis rotated by θ in the equatorial plane) and insert a $2\pi|1\rangle$-$|R\rangle$ pulse on the target qubit inside the gap as shown in Fig. 4. Performing this sequence with and without first exciting the control qubit to $|R\rangle$ with a π pulse gives an "eye" diagram that ideally consists of blockade and no-blockade curves that are π out of phase with each other. In the experiment these curves have a relative phase that is not equal to π due to Stark shifts of the qubit states induced by the Rydberg excitation beams [10]. To compensate for this we slightly detune the Rydberg pulse on the target to give the opposite phase Ramsey curves seen in the figure.

The observed amplitude of the blockade and no-blockade curves in Fig. 4 is 0.91(6) and 0.85(3). To prepare a maximally entangled Bell state with the C_Z gate the input state is $(|00\rangle + |10\rangle + |01\rangle + |11\rangle)/2$. The $|0\rangle$ state is not

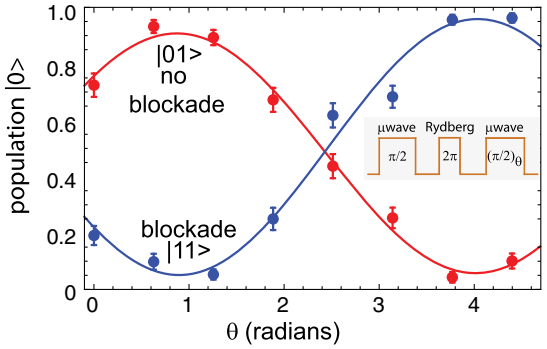

FIG. 4. Eye diagram for target qubit with blockade and no-blockade curves of amplitude 0.91(6) and 0.85(3). The inset shows the target pulse sequence. The C_Z gate was operated at $\theta = 0.95$ radians.

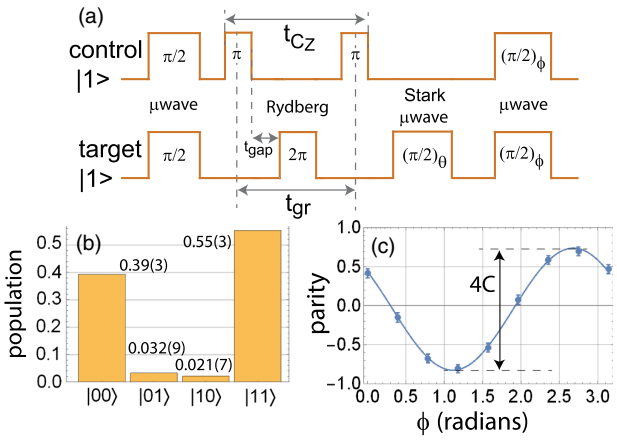

FIG. 5. Bell state preparation: (a) pulse sequence, (b) populations, (c) parity oscillation. The Rydberg pulses had lengths of $t_\pi = 150$ ns, $t_{2\pi} = 220$ ns, $t_{\text{gap}} = 300$ ns. The effective ground-Rydberg superposition time is $t_{\text{gr}} = t_\pi/2 + t_{\text{gap}} + t_{2\pi} + t_{\text{gap}} + t_\pi/2 = 0.98$ μs. The microwave pulses are global (duration 35 μs) for the initial and parity pulses and global pulses combined with a 459 nm Stark pulse (duration 70 μs) for the site selected rotation.

Rydberg coupled and is not affected by the gate sequence; therefore $|00\rangle$ experiences no error, $|10\rangle$ corresponds to Fig. 3(a), $|01\rangle$ corresponds to the no-blockade eye diagram curve, and $|11\rangle$ the blockaded eye diagram curve. The error channels discussed below in connection with Table I limit the amplitude of these curves.

To prepare a Bell state we initialize the entire array, including control and target qubits, in state $|1\rangle$ and postselect on cases when both target and control sites are filled. We do not postselect on occupation of any of the neighboring sites so the results are an average over a mean of 55% occupation. We then perform the pulse sequence shown in Fig. 5 which puts the control qubit in a superposition of $|0\rangle$ and $|1\rangle$ and implements a CNOT gate using a combination of the Rydberg C_Z and $\pi/2$ rotations on the target qubit. To simplify the pulse sequence, the initial $\pi/2$ rotations were performed with a global microwave pulse. After the C_Z, we perform a $\pi/2$ rotation of the target qubit alone about an axis θ to complete the CNOT gate [19].

The populations of the two-qubit output state are measured, and the coherence is determined from the amplitude of parity oscillations due to a global microwave $\pi/2$ rotation at variable angle ϕ [10]. The resulting data shown in Fig. 5 give $(P_{00} + P_{11})/2 = 0.47(2)$, parity amplitude $C = 0.391(6)$, and $F_{\text{Bell}} = 0.47 + 0.39 = 0.86(2)$. Note that since a global $\pi/2$ microwave pulse is used to prepare the superposition $(|00\rangle + |10\rangle + |01\rangle + |11\rangle)/2$, all atoms in the array occupy an equal superposition of $|0\rangle$ and $|1\rangle$ during the C_Z gate sequence. This superposition is representative of the average situation expected when performing a larger quantum algorithm.

The observed Bell fidelity can be understood from the error sources enumerated in Table I. The errors are divided into three categories: (a) errors due to atomic parameters, finite temperature, laser noise, and crosstalk between sites, (b) errors in the single qubit operations used for the CNOT gate and parity measurement, and (c) SPAM errors. Calculations and measurements supporting the error model are provided in the Supplemental Material [19]. The effect of each error on the output Bell state is calculated by modeling each error source as a quantum process. By propagating the input state through each of these quantum processes, we are able to accurately account for correlations between errors and the total resulting infidelity of the output Bell state [19]. Including all errors we arrive at the value in the last line of Table I which is consistent with the observed $F_{\text{Bell}} = 0.86(2)$. Accounting for SPAM errors gives a corrected Bell fidelity $F_{\text{Bell}}^{\text{-SPAM}} = 0.88$. Accounting for single qubit errors that go into the CNOT gate and parity measurements we arrive at a SPAM and single qubit gate corrected fidelity of $F_{\text{Bell}}^{C_z} = 0.89$.

Since the array filling was not deterministic, the crosstalk from neighboring sites is approximately half of what it would be in a fully occupied array. Using our error model [19], we estimate that in a deterministically loaded array we would see a reduction in Bell state fidelity of about 0.4%. Figure 1(d) shows that readout retention varies over the array with a median error that is 0.8% per atom per readout higher than the sites selected in this experiment. Using the error model [19] we estimate that the median observed Bell state fidelity for neighboring sites would be about 2.1% lower than for the sites that were used here.

The Table shows that the dominant C_Z gate errors are due to finite temperature which leads to atomic motion and dephasing, and atomic position variations in the optical traps. In addition laser intensity and phase noise contribute to the gate error at the percent level. Errors due to the finite radiative lifetime of excited states and the finite blockade strength contribute less than 1%. These observations support the potential for Rydberg gates that have fidelity compatible with fault tolerant error correction after further

technical improvements for reduced atom temperature and laser noise reduction.

In summary we have used a two-qubit Rydberg C_Z gate to create a Bell state with intrinsic fidelity after correcting for SPAM and single qubit errors of $F_{\mathrm{Bell}}^{C_Z} = 0.89$. This improved fidelity was obtained in a 2D qubit array using tightly focused control beams scanned with acousto-optic deflectors making site specific gate operations across the array possible. Therefore, the existing experimental setup allows gates on a number of sites throughout the array and provides an architecture for scaling to large quantum algorithms.

We acknowledge support from NSF PHY-1720220, the ARL-CDQI, DOE Award No. DE-SC0019465, and ColdQuanta, Inc.

Note added.—Recently, we became aware of related work demonstrating parallel operation of Rydberg gates [39].

*Present address: Joint Quantum Institute and Department of Physics, University of Maryland, College Park, Maryland 20742, USA.

†Present address: Key Laboratory of Quantum Optics, Shanghai Institute of Optics and Fine Mechanics, Chinese Academy of Sciences, Shanghai 201800, China.

‡Also at: ColdQuanta, Inc., 811 E. Washington Ave, Suite 408, Madison, Wisconsin 53703, USA.

[1] T. D. Ladd, F. Jelezko, R. Laflamme, Y. Nakamura, C. Monroe, and J. L. O'Brien, Quantum computers, Nature (London) **464**, 45 (2010).

[2] C. J. Ballance, T. P. Harty, N. M. Linke, M. A. Sepiol, and D. M. Lucas, High-Fidelity Quantum Logic Gates Using Trapped-Ion Hyperfine Qubits, Phys. Rev. Lett. **117**, 060504 (2016); J. P. Gaebler, T. R. Tan, Y. Lin, Y. Wan, R. Bowler, A. C. Keith, S. Glancy, K. Coakley, E. Knill, D. Leibfried, and D. J. Wineland, High-Fidelity Universal Gate Set for $^{9}Be^{+}$ Ion Qubits, Phys. Rev. Lett. **117**, 060505 (2016).

[3] R. Barends *et al.*, Superconducting quantum circuits at the surface code threshold for fault tolerance, Nature (London) **508**, 500 (2014).

[4] K. Wright *et al.*, Benchmarking an 11-qubit quantum computer, arXiv:1903.08181.

[5] M. Saffman, T. G. Walker, and K. Mølmer, Quantum information with Rydberg atoms, Rev. Mod. Phys. **82**, 2313 (2010).

[6] D. Jaksch, J. I. Cirac, P. Zoller, S. L. Rolston, R. Côté, and M. D. Lukin, Fast Quantum Gates for Neutral Atoms, Phys. Rev. Lett. **85**, 2208 (2000).

[7] T. Xia, M. Lichtman, K. Maller, A. W. Carr, M. J. Piotrowicz, L. Isenhower, and M. Saffman, Randomized Benchmarking of Single-Qubit Gates in a 2D Array of Neutral-Atom Qubits, Phys. Rev. Lett. **114**, 100503 (2015).

[8] Y. Wang, A. Kumar, T.-Y. Wu, and D. S. Weiss, Single-qubit gates based on targeted phase shifts in a 3D neutral atom array, Science **352**, 1562 (2016).

[9] M. Endres, H. Bernien, A. Keesling, H. Levine, E. R. Anschuetz, A. Krajenbrink, C. Senko, V. Vuletic, M. Greiner, and M. D. Lukin, Atom-by-atom assembly of defect-free one-dimensional cold atom arrays, Science **354**, 1024 (2016); D. Barredo, S. de Leséléuc, V. Lienhard, T. Lahaye, and A. Browaeys, An atom-by-atom assembler of defect-free arbitrary two-dimensional atomic arrays, Science **354**, 1021 (2016); A. Kumar, T.-Y. Wu, F. Giraldo, and D. S. Weiss, Sorting ultracold atoms in a three-dimensional optical lattice in a realization of Maxwell's demon, Nature (London) **561**, 83 (2018); D. Barredo, V. Lienhard, S. de Léséleuc, T. Lahaye, and A. Browaeys, Synthetic three-dimensional atomic structures assembled atom by atom, Nature (London) **561**, 79 (2018); D. Ohl de Mello, D. Schäffner, J. Werkmann, T. Preuschoff, L. Kohfahl, M. Schlosser, and G. Birkl, Defect-Free Assembly of 2D Clusters of more than 100 Single-Atom Quantum Systems, Phys. Rev. Lett. **122**, 203601 (2019).

[10] K. M. Maller, M. T. Lichtman, T. Xia, Y. Sun, M. J. Piotrowicz, A. W. Carr, L. Isenhower, and M. Saffman, Rydberg-blockade controlled-NOT gate and entanglement in a two-dimensional array of neutral-atom qubits, Phys. Rev. A **92**, 022336 (2015).

[11] Y.-Y. Jau, A. M. Hankin, T. Keating, I. H. Deutsch, and G. W. Biedermann, Entangling atomic spins with a Rydberg-dressed spin-flip blockade, Nat. Phys. **12**, 71 (2016).

[12] Y. Zeng, P. Xu, X. He, Y. Liu, M. Liu, J. Wang, D. J. Papoular, G. V. Shlyapnikov, and M. Zhan, Entangling Two Individual Atoms of different Isotopes via Rydberg Blockade, Phys. Rev. Lett. **119**, 160502 (2017).

[13] C. J. Picken, R. Legaie, K. McDonnell, and J. D. Pritchard, Entanglement of neutral-atom qubits with long ground-Rydberg coherence times, Quantum Sci. Technol. **4**, 015011 (2019).

[14] H. Levine, A. Keesling, A. Omran, H. Bernien, S. Schwartz, A. S. Zibrov, M. Endres, M. Greiner, V. Vuletić, and M. D. Lukin, High-Fidelity Control and Entanglement of Rydberg-Atom Qubits, Phys. Rev. Lett. **121**, 123603 (2018).

[15] C. Sheng, X. He, P. Xu, R. Guo, K. Wang, Z. Xiong, M. Liu, J. Wang, and M. Zhan, High-Fidelity Single-Qubit Gates on Neutral Atoms in a Two-Dimensional Magic-Intensity Optical Dipole Trap Array, Phys. Rev. Lett. **121**, 240501 (2018).

[16] M. J. Piotrowicz, M. Lichtman, K. Maller, G. Li, S. Zhang, L. Isenhower, and M. Saffman, Two-dimensional lattice of blue-detuned atom traps using a projected Gaussian beam array, Phys. Rev. A **88**, 013420 (2013).

[17] M. T. Lichtman, Coherent operations, entanglement, and progress towards quantum search in a large 2D array of neutral atom qubits, Ph.D. thesis, University of Wisconsin-Madison, 2015.

[18] T. Graham *et al.* (to be published).

[19] See Supplemental Material at http://link.aps.org/supplemental/10.1103/PhysRevLett.123.230501 for an experimental setup diagram, an explanation of error sources, details of process matrix error modeling, and a simulation

of decoherence in Rabi oscillations, which includes Refs. [5,7,10,14,17,18,20–33].

[20] S. de Léséleuc, D. Barredo, V. Lienhard, A. Browaeys, and T. Lahaye, Analysis of imperfections in the coherent optical excitation of single atoms to Rydberg states, Phys. Rev. A **97**, 053803 (2018).

[21] X. L. Zhang, A. T. Gill, L. Isenhower, T. G. Walker, and M. Saffman, Fidelity of a Rydberg blockade quantum gate from simulated quantum process tomography, Phys. Rev. A **85**, 042310 (2012).

[22] X. L. Zhang, L. Isenhower, A. T. Gill, T. G. Walker, and M. Saffman, Deterministic entanglement of two neutral atoms via Rydberg blockade, Phys. Rev. A **82**, 030306(R) (2010).

[23] T. Wilk, A. Gaëtan, C. Evellin, J. Wolters, Y. Miroshnychenko, P. Grangier, and A. Browaeys, Entanglement of Two Individual Neutral Atoms Using Rydberg Blockade, Phys. Rev. Lett. **104**, 010502 (2010).

[24] M. Saffman and T. G. Walker, Analysis of a quantum logic device based on dipole-dipole interactions of optically trapped Rydberg atoms, Phys. Rev. A **72**, 022347 (2005).

[25] M. Saffman, X. L. Zhang, A. T. Gill, L. Isenhower, and T. G. Walker, Rydberg state mediated quantum gates and entanglement of pairs of neutral atoms, J. Phys. Conf. Ser. **264**, 012023 (2011).

[26] K. Gillen-Christandl, G. Gillen, M. J. Piotrowicz, and M. Saffman, Comparison of Gaussian and super Gaussian laser beams for addressing atomic qubits, Appl. Phys. B **122**, 131 (2016).

[27] I. I. Beterov, I. I. Ryabtsev, D. B. Tretyakov, and V. M. Entin, Quasiclassical calculations of blackbody-radiation-induced depopulation rates and effective lifetimes of Rydberg nS, nP, and nD alkali-metal atoms with $n <= 80$, Phys. Rev. A **79**, 052504 (2009).

[28] I. I. Beterov, I. I. Ryabtsev, D. B. Tretyakov, and V. M. Entin, Erratum: Quasiclassical calculations of blackbody-radiation-induced depopulation rates and effective lifetimes of Rydberg nS, nP, and nD alkali-metal atoms with $n <= 80$, Phys. Rev. A **80**, 059902(E) (2009).

[29] I. I. Beterov, M. Saffman, E. A. Yakshina, V. P. Zhukov, D. B. Tretyakov, V. M. Entin, I. I. Ryabtsev, C. W. Mansell, C. MacCormick, S. Bergamini, and M. P. Fedoruk, Quantum gates in mesoscopic atomic ensembles based on adiabatic passage and Rydberg blockade, Phys. Rev. A **88**, 010303(R) (2013).

[30] M. Kwon, M. F. Ebert, T. G. Walker, and M. Saffman, Parallel Low-Loss Measurement of Multiple Atomic Qubits, Phys. Rev. Lett. **119**, 180504 (2017).

[31] P. Rosenbusch, S. Ghezali, V. A. Dzuba, V. V. Flambaum, K. Beloy, and A. Derevianko, ac Stark shift of the Cs microwave atomic clock transitions, Phys. Rev. A **79**, 013404 (2009).

[32] A. W. Carr and M. Saffman, Doubly Magic Optical Trapping for Cs Atom Hyperfine Clock Transitions, Phys. Rev. Lett. **117**, 150801 (2016).

[33] S. Kuhr, W. Alt, D. Schrader, I. Dotsenko, Y. Miroshnychenko, A. Rauschenbeutel, and D. Meschede, Analysis of dephasing mechanisms in a standing-wave dipole trap, Phys. Rev. A **72**, 023406 (2005).

[34] S. Zhang, F. Robicheaux, and M. Saffman, Magic-wavelength optical traps for Rydberg atoms, Phys. Rev. A **84**, 043408 (2011).

[35] S. Zhang, Trapping and Rydberg excitation of a single atom qubit in a blue detuned bottle beam, Ph.D. thesis, University of Wisconsin-Madison, 2012.

[36] Our expression for $T_{2,\mathrm{D}}$ is $\sqrt{2}$ larger than that in [23] where this dephasing mechanism was first pointed out.

[37] M. Saffman, Quantum computing with atomic qubits and Rydberg interactions: Progress and challenges, J. Phys. B **49**, 202001 (2016).

[38] L. S. Theis, F. Motzoi, F. K. Wilhelm, and M. Saffman, A high fidelity Rydberg blockade entangling gate using shaped and analytic pulses, Phys. Rev. A **94**, 032306 (2016).

[39] H. Levine, A. Keesling, G. Semeghini, A. Omran, T. T. Wang, S. Ebadi, H. Bernien, M. Greiner, V. Vuletić, H. Pichler, and M. D. Lukin, Parallel Implementation of High-Fidelity Multi-Qubit Gates with Neutral Atoms, Phys. Rev. Lett. **123**, 170503 (2019).